VNU Journal of Science: Mathematics - Physics
Journal homepage: https://js.vnu.edu.vn/MaP

Original Article

Synthesis of Tungsten Oxide Nanofibers Using Electrospinning Towards Gas Sensor Application

Do Hoang Yen[1,2], Le Tran Ngoc Phu[1,2], Dang Thi Thanh Le[1,2,*]

[1]*Faculty of Electronic Materials and Devices, School of Materials Science and Engineering (SMSE), Hanoi University of Science and Technology (HUST), 1 Dai Co Viet, Hanoi, Vietnam*
[2]*International Training Institute for Materials Science (ITIMS), Hanoi University of Science and Technology (HUST), 1 Dai Co Viet, Hanoi, Vietnam*

Received 4th March 2025
Revised 18th April 2025; Accepted 20th June 2025

Abstract: A simple strategy was introduced to synthesize WO_3 nanofibers through an electrospinning process. In this work, tungstic acid, hydrogen peroxide and polyvinyl pyrrolidone were used as precursors. After electrospinning and drying the desired material was collected. The morphology and structure of the samples were analyzed by field-emission scanning electron microscopy (FESEM), energy-dispersive x-ray spectroscopy (EDS) mapping, and X-ray diffraction (XRD). The results show that the obtained materials are composed by nanofibers with uniform dimensions. The first tests of ammonia sensing were done from 250 to 450 °C; the WO_3 NFs sensor presented a good response of 3.48 to 500 ppm NH_3 at an operation temperature of 450 °C.

Keywords: WO_3, nanofibers, electrospinning, NH_3, gas sensor.

1. Introduction

Gas sensors are essential tools for real-time air quality monitoring, playing a vital role in addressing air pollution. These devices are classified basing on the types of utilized materials, such as metal oxide semiconductors (SMOs), polymers, solid electrolytes, and other categories. Among these, TiO_2 [1], SnO_2 [2], ZnO [3], Co_3O_4 [4], In_2O_3 [5] and WO_3 [6] have attracted considerable interest due to their ease of fabrication and fast response times. The operation of gas sensors is based on the interaction between the sensing material and the target gas, which results in a change in the sensor's resistance.

* Corresponding author.
E-mail address: thanhle@itims.edu.vn

https//doi.org/10.25073/2588-1124/vnumap.4993

Specifically, the sensing performance of semiconductor metal oxides is influenced by factors like morphology and particle size, both of which are dependenton both the fabrication method and experimental conditions.

Significant advancements in the synthesis of nanomaterials have been achieved over the past decades, with transition metal oxides becoming a prominent area of research. The microscopic morphology of these materials is crucial in shaping their properties. Presently, synthesized transition metal oxides exhibit one-, two-, and three-dimensional structures. Notably, one-dimensional (1D) nanostructures are particularly advantageous for sensor application [7, 8] due to their well-controlled morphology, ease of fabrication, high surface-to-volume ratio, abundant surface-active sites, and intrinsic semiconductor properties. These characteristics render them more sensitive than other materials. Considerable efforts have been made to develop 1D sensing nanomaterials through various fabrication methods, such as thermal oxidation, thermal evaporation, self-catalytic growth, molten salt synthesis, and electrospinning [9, 10]. Among these, electrospinning has gained notable attention for its simplicity and versatility, enabling the production of 1D nanomaterials with a high length-to-diameter ratio, which enhances electron transport efficiency [11, 12].

Tungsten oxide (WO_3) is a representative n-type semiconductor that demonstrates excellent suitability for gas sensing applications. This is attributed to its high chemical stability, non-toxicity, favorable electronic mobility, wide bandgap (E_g = 2.5–3.0 eV), pronounced resistance variation during gas exposure, and cost-effectiveness [13-15]. Gas sensing performance is predominantly governed by surface reaction mechanisms on active materials. Consequently, the morphology of the sensing material – encompassing attributes such as surface area, porosity, and active site distribution – is a critical factor in determining its overall gas sensing properties. Therefore, the morphology of the sensing material will play a defining role on the resultant gas sensing properties. Nanostructured SMOs featuring engineered morphologies and intrinsic porosity have demonstrated exceptional efficacy in enhancing gas sensing performance [6]. Electrospun one-dimensional WO_3 nanostructures, such as nanofibers [16] and nanotubes [17] demonstrate superior gas sensing performance, primarily due to their high porosity and the interconnectivity of constituent nanoparticles. WO_3 nanofibers were studied for detecting many gases such as hydrogen [18], triethylamine [19], and acetone [6]. Significant progress has been achieved in the design and synthesis of WO_3 nanostructures across various dimensions to optimize their gas sensing properties.

In this work, WO_3 nanofibers (NFs) were fabricated through electrospinning technique, and their properties were characterized using field-emission scanning electron microscopy (FESEM), X-ray diffraction (XRD), and energy-dispersive X-ray spectroscopy (EDS) mapping. The gas-sensing performance of the prepared WO_3 material towards ammonia was evaluated.

2. Experimental

Tungstic acid (H_2WO_4, Sigma-Aldrich, ≥ 98%), polyvinyl pyrrolidone (PVP, Mw = 40,000), hydrogen peroxide H_2O_2 and ethanol (Sigma-Aldrich) were all used as received without further purification.

First, two solution containers for electrospinning were prepared simultaneously, the first container was used to dissolve polyvinyl pyrrolidone in 5.5 ml ethanol (to get solution A), while the second container contained 3.5 ml H_2O_2 to dissolve 0.8 g H_2WO_4 (to get solution B). Both containers were stirred vigorously at the same rotation speed and at 120 ^oC, they were rotated for 1 h and 2 h, respectively. Then, mixing and stirring vigorously both solutions for 1 ah at 120 ^oC to produce PVP/H_2WO_4 solution (solution C). Later, PVP/H_2WO_4 solution was loaded into a 10 mL plastic syringe with a needle gauge size of 21 G after 1 h cooling down process. The nanofibers were formed under

high voltage of 21 kV during the electrospinning process. In the experimental setup, the needle serves as the anode and the collector functions as the cathode. The gap between the needle and collector was fixed at 10 cm, while the solution was delivered at a controlled flow rate of 0.008 $mL.min^{-1}$. Additionally, the mandrel was rotated at a constant speed of 400 rpm. Then the obtained material was dried at 60 °C for 3 hours. Finally, use an alumina boat to contain the obtained material and placed into a tubular furnace for calcination at 500 °C for 2 h.

The as-prepared and the annealed nanofibers were characterized and analyzed by using X-ray diffraction (XRD, field-emission scanning electron microscopy (FESEM, and energy dispersive spectrometry (EDS). The XRD analysis was performed using a Bruker D5005 X-ray diffractometer with CuKα1 radiation (λ = 1.5406 Å) at 40 kV and 40 mA. FESEM images were obtained using a JEOL7600 scanning electron microscope at an accelerating voltage of 20 kV.

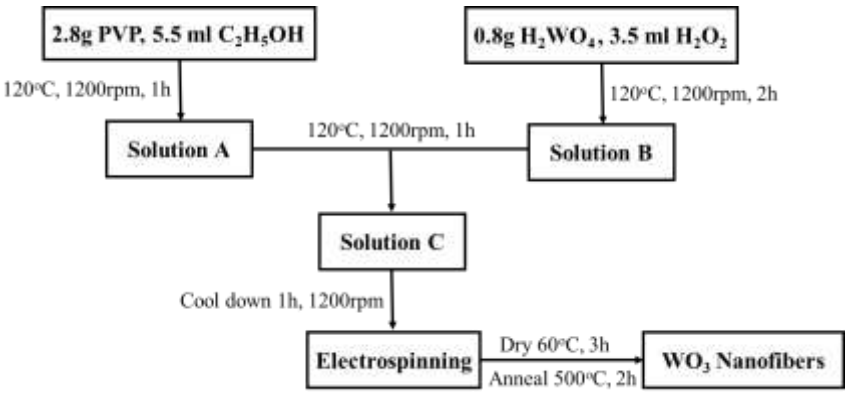

Figure 1. Preparation procedure of WO_3 nanofibers.

The synthesized material was uniformly electrospun onto silicon substrates coated with interdigitated platinum electrodes to form a robust sensing thick layer. Subsequently, the sensor was annealed in air at 500 °C for 2 h to enhance both the material's stability and its adhesion to the electrodes. Electrical resistance was continuously monitored using a Keithley 2602 source meter during cyclic exposures to ammonia diluted in air, with precise gas flow control provided by MKS model GV50 mass flow controllers. Pulses of the analyte gas, with concentrations ranging from 25 to 500 ppm, were introduced while maintaining a constant total gas flow of 400 sccm. Measurements were conducted over a temperature span of 250 °C to 450 °C in 50 °C steps-up using a custom-built system. For this n-type metal oxide semiconductor sensor, exposure to reducing gases leads to an increase in resistance, and sensor response is quantified as $S = R_a/R_g$, where R_a and R_g represent the stabilized resistance of the sensor in air and in the presence of the target gas, respectively.

3. Results and Discussion

3.1. Nanofiber Characterization

The morphological features of WO_3 nanostructures were investigated using scanning electron microscopy (SEM). As illustrated in Fig. 2, the H_2WO_4/PVP composite nanofibers were observed to form nonwoven mats with randomly oriented structures.

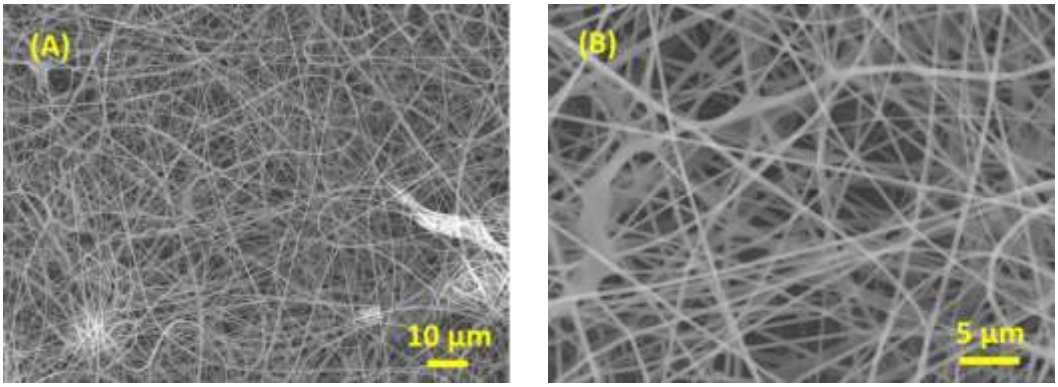

Figure 2. SEM images of as-prepared H_2WO_4/PVP composite nanofibers at diverse magnifications: A) low magnification and B) high magnification.

This particular arrangement is attributed to the bending instability experienced by the spinning jet during the electrospinning process. Each individual fiber exhibited a uniform and smooth cross-section, characterized by an average diameter of approximately 300 - 500 nm. The surface of the WO_3 nanofibers displayed bending patterns and exhibited overall smoothness.

Subsequently, the precursor fibers were subjected to controlled heating at a rate of 1 °C per minute until 500 °C. Fig. 3 displays the SEM images, showcasing the presence of numerous nanofibers, extending up to tens of microns in length. These nanofibers displayed a random and intertwined stacking pattern. Upon the formation of WO_3, the average diameter of the nanofibers decreased to approximately 50 - 150 nm, with the constituent particles, as shown in Fig. 3(B). These changes in morphologies can be attributed to the degradation of PVP at high temperatures, leading to the transformation of the precursor nanofibers into the final WO_3 nanofibers.

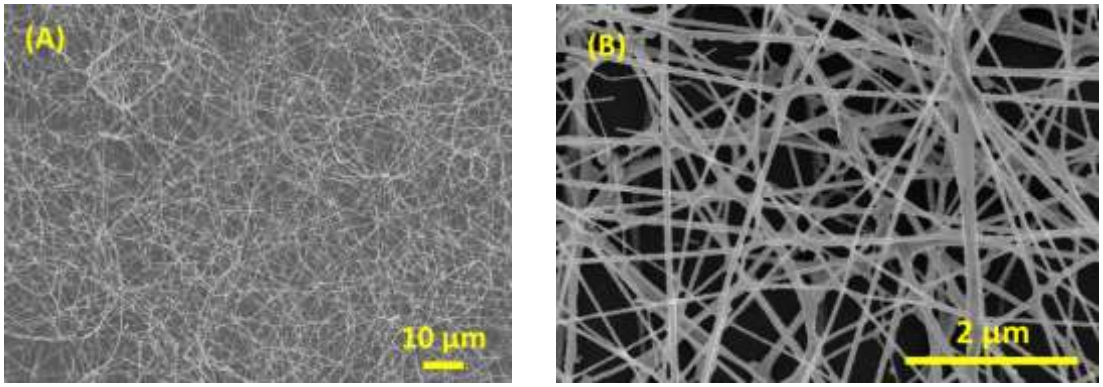

Figure 3. SEM image (A) and FESEM image (B) of annealed WO_3 nanofibers.

The composition of the annealed sample was thoroughly investigated using Energy Dispersive Spectrometry (EDS) and EDS mapping, as depicted in Fig. 4. The EDS elemental spectrum in Fig. 5d confirms the presence of W and O elements within the sample. The distribution of W and O elements was found to be uniform throughout the entire obtained nanofibers, as evidenced by the EDS mapping in Figs. 4(B) and 4(C). These analytical results provide valuable insights into the elemental composition and distribution within the annealed nanofibers, contributing to a comprehensive understanding of the material's structure and properties.

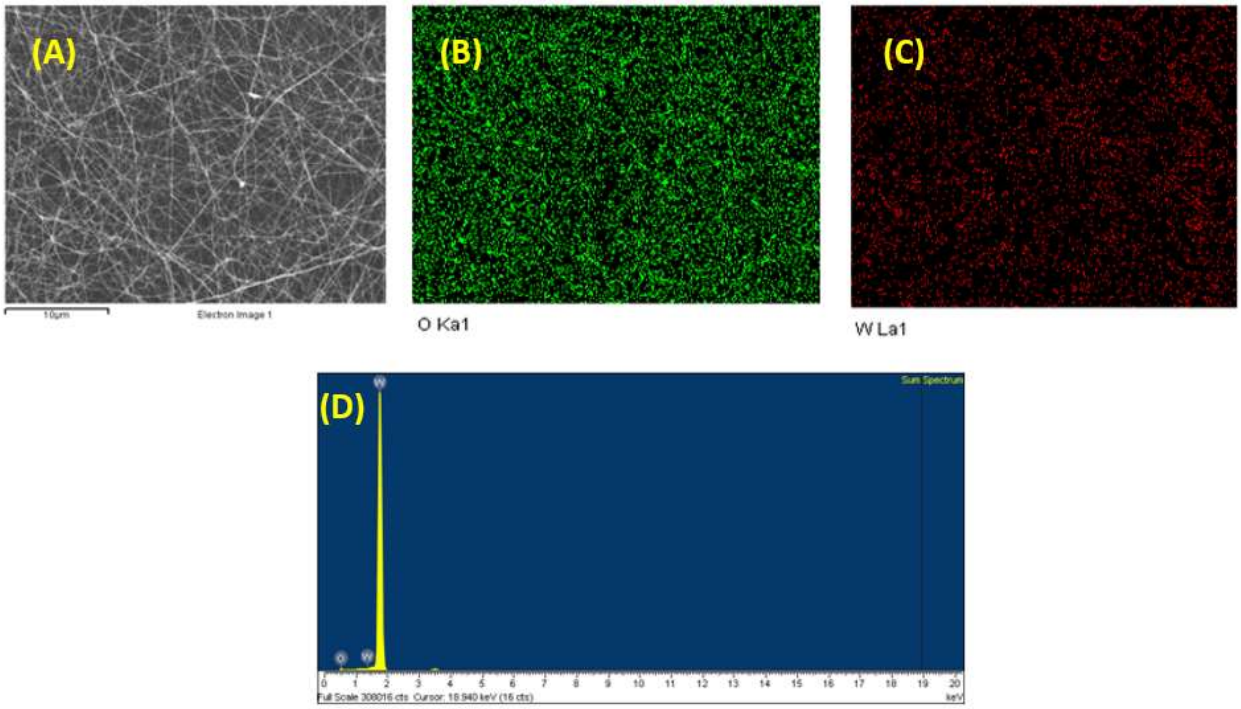

Figure 4. SEM image (A), EDS spectrum (D) of WO_3 nanofibers and EDS mapping of O (B) and W (C) element.

The crystalline structure of the synthesized WO_3 nanofibers was analyzed using X-ray diffraction, as shown in Fig. 5. The diffraction patterns exhibit characteristic peaks at 23.2°, 23.7°, 24.5°, 26.8°, 28.9°, 33.4°, 34.2°, 35.7°, 41.8°, 45.3°, 47.4°, 48.4°, 50.1°, 53.7°, 55.9°, 60.2° and 62.2° which correspond to the (002), (020), (200), (120), ($\bar{1}$12), (022), (202), ($\bar{1}$22), (222), (132), (004), (040), (400), (114), ($\bar{2}$04), (420), (242), and (340) crystallographic planes. These reflections are in good agreement with the monoclinic phase of WO_3, as indexed by the JCPDS Card No. 83-0950 [16].

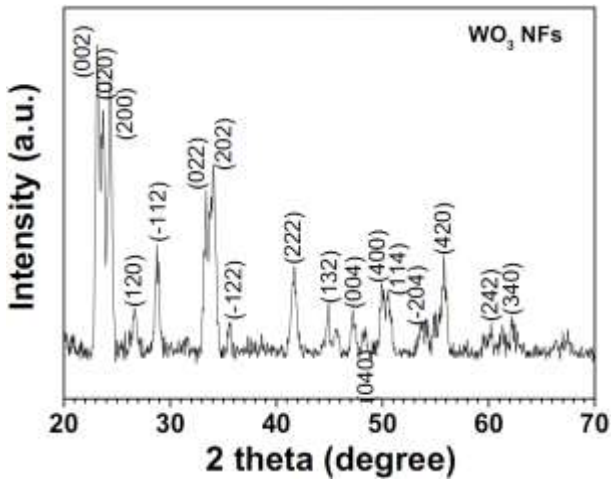

Figure. 5. XRD patterns of WO_3 nanofibers.

3.2. Gas Sensing Property

For ammonia sensing investigations, WO_3 nanofibers, annealed at 500 °C for 2 h, were selected as the sensing material. The time-dependent response alterations of the WO_3 sensor were surveyed while operating at various operating temperatures and subjected to varying concentrations of NH_3 gas (25, 50, 100, 250, and 500 ppm). The results, illustrated in Fig. 6, furnish valuable insights into the gas sensitivity of WO_3 materials towards NH_3.

Fig. 6a illustrates five real-time response profiles of the WO_3 nanofiber sensor while operating at various working temperatures. Upon exposure to NH_3 gas, the sensor exhibited an increase in response, subsequently reverting to its initial state upon the removal of the gas source. This behavior is indicative of the n-type semiconductor characteristics inherent to the WO_3 material.

Fig. 6b presents the response data derived from Fig. 6a. These results underline that at the operational temperature of 450 °C, the WO_3 sensor demonstrated its highest sensitivity when exposed to 500 ppm NH_3 gas, exhibiting a response value (S) of 3.48. For NH_3 concentrations of 25, 50, 100, and 250 ppm, the response values were 1.88, 2.29, 2.4, and 2.79, respectively. It is noteworthy that the sensor's response exhibited an upward trend in parallel with increasing gas concentration.

WO_3 is a widely recognized n-type semiconductor, a property typically exhibited under standard fabrication conditions. However, when WO_3 nanofibers are exposed to ambient air, oxygen molecules have tend to adsorb onto their surface, adopting the form of O^- and O^{2-} ions as the following equations (1) and (2):

$$O_2 + e^- \rightarrow O^- \quad (1)$$

$$O_2 + e^- \rightarrow O^{2-} \quad (2)$$

This phenomenon leads to a substantial coverage of adsorbed oxygen ions, which in turn sequester electrons within the nanostructure, thereby diminishing their availability and impairing electrical conductivity under these circumstances. Upon the introduction of ammonia into the sensor devices, the ammonia molecules engage in chemical reactions (3) and (4) with the adsorbed oxygen species as below:

$$2NH_3 + 3O^- \rightarrow N_2 + 3H_2O + 3e^- \quad (3)$$

$$2NH_3 + O^{2-} \rightarrow N_2 + 3H_2O + 2e^- \quad (4)$$

This interaction triggers the liberation of previously trapped electrons, facilitating their return to the nanofiber layer. Consequently, this process augments the electron population within the material, yielding a concurrent augmentation in sensor response.

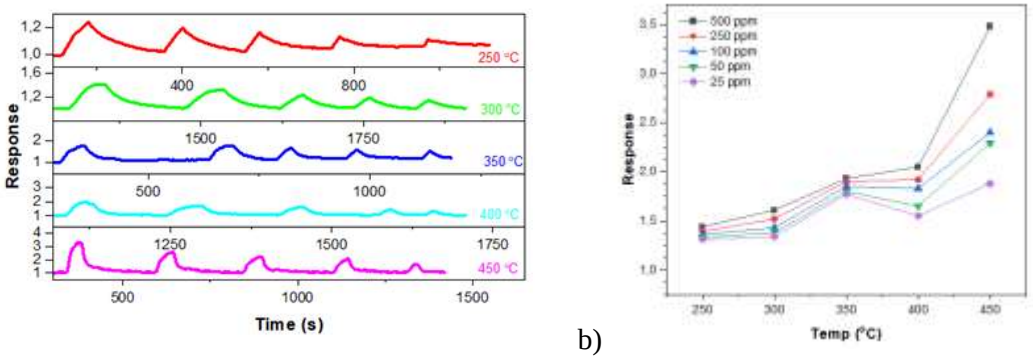

a) b)

Figure 6. The response of the WO_3 sensor to NH_3 gas: (a) Transient response as a function of time spanning concentrations from 25 to 500 ppm at different operation temperatures, (b) Response behavior across a range of concentrations from 25 to 500 ppm, at different working temperatures.

Table 1. The comparison of ammonia sensing performance of WO_3 nanomaterials in recent literature

Material	Temperature (°C)	Concentration (ppm)	Response	Reference
WO_3 thin film	250	100	1.25	[20] (2024)
WO_3 thin film	250	500	2.67	[21] (2023)
MoS_2/WO_3 nanosheets	200	200	2.07	[22] (2021)
WO_3 thin film	300	1000	1.8	[23] (2017)
WO_3 NFs	450	100	2.4	This study

To assess the gas sensing performance of the synthesized WO_3 nanofibers, we performed a comparative analysis with previously reported studies, with the results summarized in Table 1. The data indicate that our sensor performs better property in detecting NH_3 compared to earlier reported devices.

4. Conclusion

In this work, WO_3 nanofibers were prepared by an electrospinning method. The obatined results showed that WO_3 nanofibers have porous structures composed of nanoparticles. Their ammonia sensing property was also tested. The sensor exhibits a good response of 3.48 to 500 ppm NH_3 at the operating temperature of 450 °C. The results demonstrate the successful fabrication of WO_3 nanofibers with uniform dimensions and highlight their potential for NH_3 sensing application.

Acknowledgments

This research is funded by Vietnam National Foundation for Science and Technology Development (NAFOSTED) under grant number 103.02-2021.36.

References

[1] V. Galstyan, A. Ponzoni, I. Kholmanov, M.M. Natile, E. Comini, S. Nematov, G. Sberveglieri, Investigation of Reduced Graphene Oxide and a Nb-Doped TiO_2 Nanotube Hybrid Structure to Improve the Gas-Sensing Response and Selectivity, ACS Sensors, Vol. 4, 2019, pp. 2094-2100, https://doi.org/10.1021/acssensors.9b00772.

[2] T. Wang, Q. Xing, R. Zhai, T. Huang, P. Song, Defect Engineering for SnO_2 Improves NO_2 Gas Sensitivity by Plasma Spraying, ACS Sensors, Vol. 9, 2024, pp. 3178-3186, https://doi.org/10.1021/acssensors.4c00485.

[3] Y. Kang, F. Yu, L. Zhang, W. Wang, L. Chen, Y. Li, Review of ZnO-based Nanomaterials in Gas Sensors, Solid State Ionics, Vol. 360, 2021, pp. 115544, https://doi.org/10.1016/j.ssi.2020.115544.

[4] T. T. Le Dang, T. N. T. Do, V. M. Do, M. Tonezzer, V. D. N. Tran, T. X. Chu, M. H. Chu, V. D. Nguyen, D. H. Nguyen, Eco-friendly Facile Synthesis of Co_3O_4–Pt Nanorods for Ethylene Detection towards Fruit Quality Monitoring, Sensors and Actuators A: Physical, Vol. 362, 2023, pp. 114607, https://doi.org/10.1016/j.sna.2023.114607.

[5] N. H. Tan, D. T. T. Le, T.T. Hoang, N. M. Duy, M. Tonezzer, C. T. Xuan, N. V. Duy, N. D. Hoa, Metal-decorated Indium Oxide Nanofibers Used as Nanosensor for Triethylamine Sensing towards Seafood Quality Monitoring, Colloids Surfaces A Physicochemical Engineering Aspects, Vol. 703, 2024, pp. 135268, https://doi.org/10.1016/j.colsurfa.2024.135268.

[6] J. Zhang, T. Shao, J. Dong, G. Li, J. Liu, Y. Liu, R. Yang, J. Gao, L. Li, Y. Jia, L. Zhang, H. Lu, Construction of Mesoporous WO_3 Nanofibers Functionalized with Nanoscale PtO Catalysts for Enhanced Acetone Sensing Properties, J. Alloys Compounds, Vol. 933, 2023, pp. 2-10, https://doi.org/10.1016/j.jallcom.2022.167703.

[7] I. Cho, J. Ko, D. D. O. Henriquez, D. Yang, I. Park, Recent Advances in 1D Nanostructure Assembly and Direct Integration Methods for Device Applications, Small Methods, Vol. 2400474, 2024, pp. 1-30, https://doi.org/10.1002/smtd.202400474.

[8] T. Li, W. Zeng, Z. Wang, Quasi-one-dimensional Metal-oxide-based Heterostructural Gas-sensing Materials: A Review, Sensors and Actuators B: Chemical, Vol. 221, 2015, pp. 1570-1585, https://doi.org/10.1016/j.snb.2015.08.003.

[9] E. Comini, C. Baratto, G. Faglia, M. Ferroni, A. Vomiero, G. Sberveglieri, Quasi-one Dimensional Metal Oxide Semiconductors: Preparation, Characterization and Application as Chemical Sensors, Progress in Materials Science, Vol. 54, 2009, pp. 1-67, https://doi.org/10.1016/j.pmatsci.2008.06.003.

[10] C. I. Ossai, N. Raghavan, Nanostructure and Nanomaterial Characterization, Growth Mechanisms, and Applications, Nanotechnology Review, Vol. 7, 2018, pp. 209-231, https://doi.org/10.1515/ntrev-2017-0156.

[11] W. Smok, T. Tański, A Short Review on Various Engineering Applications of Electrospun One-Dimensional Metal Oxides, Materials (Basel), Vol. 14, 2021, pp. 5139, https://doi.org/10.3390/ma14185139.

[12] P. Karnati, S. Akbar, P. A. Morris, Conduction Mechanisms in One Dimensional Core-shell Nanostructures for Gas Sensing: A Review, Sensors and Actuators B: Chemical, Vol. 295, 2019, pp. 127-143, https://doi.org/10.1016/j.snb.2019.05.049.

[13] J. Zhang, D. Leng, L. Zhang, G. Li, F. Ma, J. Gao, H. Lu, B. Zhu, Porosity and Oxygen Vacancy Engineering of Mesoporous WO_3 Nanofibers for Fast and Sensitive Low-Temperature NO_2 Sensing, J. Alloys and Compounds, Vol. 853, 2021, pp. 157339, https://doi.org/10.1016/j.jallcom.2020.157339.

[14] M. Punginsang, D. Zappa, E. Comini, A. Wisitsoraat, G. Sberveglieri, A. Ponzoni, C. Liewhiran, Selective H_2S Gas Sensors Based on Ohmic Hetero-Interface of Au-Functionalized WO_3 Nanowires, Applied Surface Science, Vol. 571, 2022, pp. 151262, https://doi.org/10.1016/j.apsusc.2021.151262.

[15] X. Y. Yang, J. Y. Yuan, L. J. Yue, K. F. Xie, F. L. Gong, S. Z. Wei, Y. H. Zhang, Electronic and Surface Structure Engineering of Oxygen Vacancies-Riched WO_3 Nanosheets toward Highly Efficient BTEX Sensing, Sensors and Actuators B: Chemical, Vol. 405, 2024, pp. 135357, https://doi.org/10.1016/j.snb.2024.135357.

[16] Y. Qiu, Y. Wang, Synthesis, Growth Kinetics and Ultra-sensitive Performance of Electrospun WO_3 Nanofibers for NO_2 Detection, Applied Surface Science, Vol. 608, 2023, pp. 155112, https://doi.org/10.1016/j.apsusc.2022.155112.

[17] S. Zeb, X. Peng, G. Yuan, X. Zhao, C. Qin, G. Sun, Y. Nie, Y. Cui, X. Jiang, Controllable Synthesis of Ultrathin WO_3 Nanotubes and Nanowires with Excellent Gas Sensing Performance, Sensors and Actuators B: Chemical, Vol. 305, 2020, pp. 127435, https://doi.org/10.1016/j.snb.2019.127435.

[18] J. Li, X. Mo, K. Zhang, S. Ali, Z. Liu, P. Cheng, Y. Li, K. Sun, Y. Fu, Y. Wang, E. Xie, Ru Modulates the Catalytic Activity of Pt to Modify WO_3 Nanowires for High-performance Hydrogen Sensing at Near Room Temperature, Applied Surface Science, Vol. 615, 2023, pp. 156286, https://doi.org/10.1016/j.apsusc.2022.156286.

[19] S. Zhang, B. Zhang, W. Li, Y. Dong, Y. Ni, P. Yu, J. Liang, N. Y. Kim, J. Wang, Electrospun Copper-doped Tungsten Oxide Nanowires for Triethylamine Gas Sensing, Vacuum, Vol. 215, 2023, pp. 112377, https://doi.org/10.1016/j.vacuum.2023.112377.

[20] S. Singh, P. Gurawal, G. Malik, R. Adalati, D. Kaur, R. Chandra, Highly Responsive and Selective NO Gas Sensing Based on Room Temperature Sputtered Nanocrystalline WO_3/Si Thin Films, Micro and Nanostructures. Vol. 188, 2024, pp. 207794, https://doi.org/10.1016/j.micrna.2024.207794.

[21] A. Yadav, A. Sharma, V. Baloria, P. Singh, G. Gupta, Ultrahigh Sensitive NO Sensor Based on WO_3 Film with Ppb-level Sensitivity, Ceramics International, Vol. 49, 2023, pp. 7853-7860, https://doi.org/10.1016/j.ceramint.2022.10.284.

[22] S. Singh, J. Deb, U. Sarkar, S. Sharma, MoS_2/WO_3 Nanosheets for Detection of Ammonia, ACS Applied Nano Materials, Vol. 4, 2021, pp. 2594-2605, https://doi.org/10.1021/acsanm.0c03239.

[23] N. V. Toan, C. M. Hung, N. V. Duy, N. D. Hoa, D. T. T. Le, N. V. Hieu, Bilayer SnO_2–WO_3 Nanofilms for Enhanced NH_3 Gas Sensing Performance, Materials Science and Engineering B: Solid-State Materials Advanced Technology, Vol. 224, 2017, pp. 163-170, https://doi.org/10.1016/j.mseb.2017.08.004.